BBA - General Subjects 1865 (2021) 129918

Contents lists available at ScienceDirect

BBA - General Subjects

journal homepage: www.elsevier.com/locate/bbagen

An atomic perspective on improving daptomycin's activity

Pilar Blasco [a,1], Chunlei Zhang [a,1], Hoi Yee Chow [a], Guanhua Chen [a], Yongsheng Wu [c], Xuechen Li [a,b,*]

[a] Department of Chemistry, State Key Lab of Synthetic Chemistry, The University of Hong Kong, Pokfulam Road, Hong Kong
[b] Laboratory for Marine Drugs and Bioproducts, Qingdao National Laboratory for Marine Science and Technology, Qingdao, PR China
[c] Mudanjiang YouBo Pharmaceutical Co., Ltd, Mudanjiang, PR China

ARTICLE INFO

Keywords:
Daptomycin
Calcium dependent antibiotics
Oligomerization
Nuclear magnetic resonance (NMR)
Molecular dynamics (MD)
Cyclic peptide

ABSTRACT

Background: Recently, through comprehensive medicinal chemistry efforts, we have found a new daptomycin analogue, termed kynomycin, showing enhanced activity against both methicillin-resistant *S. aureus* and vancomycin-resistant *Enterococcus* in vitro and in vivo, with improved pharmacokinetics and lower cytotoxicity than daptomycin.
Methods: In this study we compared the physicochemical properties of kynomycin with those of daptomycin from an atomic perspective by using Nuclear Magnetic Resonance spectroscopy and Molecular Dynamics simulations.
Results and conclusion: We observed that kynurenine methylation changes daptomycin's key physicochemical properties; its calcium dependent oligomerization efficiency is improved and the modified kynurenine strengths contacts with the lipid tail and tryptophan residues. In addition, it is observed that, compared to daptomycin, kynomycin tetramer is more stable and binds stronger to calcium. The combined experiments provide key clues for the improved antibacterial activity of kynomycin.
General significance: We expect that this approach will help study the calcium binding and oligomerization features of new calcium dependent peptide antibiotics.

1. Introduction

Daptomycin is one of the few antibacterial agents developed to treat Gram-positive based skin infections and the first-in-class cyclic lipopeptide antibiotic in clinical use since 2003 [1]. The drug exhibits significant bactericidal activity against drug-resistant Gram-positive bacterial strains, including methicillin- and vancomycin-resistant *S. aureus* (MRSA and VRSA) and VRE [2–4]. However, the number of daptomycin resistant bacterial pathogens has increased at an alarming rate [5,6], thus there is an urgent need to fight back and develop a new-generation of daptomycin-based antibiotics.

Despite daptomycin has been used in clinical for almost 20 years, its unique mode of action (MOA) remained uncertain. Recent reports follow a more similar path on the MOA: daptomycin undergoes calcium (Ca^{2+}) induced oligomerization into micro-micelles which deliver it to the bacterial membrane at high localized concentrations [7–9]. When near to the bacterial membrane, the oligomer dissociates and penetrates the membrane bilayer, where it reassembles into channels leading to membrane depolarization and consequent cell death [10–12]. However, several of these key steps are not completely understood and therefore still highly controversial; different theories have been recently proposed showing that the MOA remains unclear [13–16].

Various research groups have established the structure-activity relationship (SAR) of daptomycin and produced analogues by semi-synthesis, chemo-enzymatic, combinatorial biosynthesis and total chemical synthesis [17–23]. We recently have performed a detailed SAR analysis on daptomycin and obtained 80 analogues via chemical synthesis [24], from where we have observed that methylations of specific amino acids (Trp1, Gly5 and Kyn13) enhanced the daptomycin's antibacterial effect. In particular, the aniline group's methylation at Kyn13 in daptomycin showed the most dramatic effect on the activity, superior to that of daptomycin. Kynomycin eradicated both daptomycin-sensitive and -resistant MRSA and VRE in vitro and in vivo, and showed improved pharmacokinetics and lower cytotoxicity than daptomycin [25].

In this work, we analysed and compared the physicochemical properties of kynomycin and daptomycin from an atomic perspective by

* Corresponding author at: Department of Chemistry, State Key Lab of Synthetic Chemistry, The University of Hong Kong, Pokfulam Road, Hong Kong.
E-mail address: xuechenl@hku.hk (X. Li).
[1] Contributed equally.

https://doi.org/10.1016/j.bbagen.2021.129918
Received 1 January 2021; Received in revised form 3 May 2021; Accepted 3 May 2021
Available online 13 May 2021

using a combination of Nuclear Magnetic Resonance (NMR) spectroscopy and Molecular Dynamics (MD) simulations. By using Ca^{2+} titration experiments and the analysis of different NMR parameters, the oligomerization of both daptomycin and kynomycin in the presence of Ca^{2+} and the peptide local conformation were studied. In addition, kynomycin's tetramer stability and binding to Ca^{2+} were calculated from the MD simulations. Overall, we have demonstrated that the methylation of Kyn13 changed kynomycin's key physicochemical properties as compared to daptomycin.

2. Results

2.1. Kynomycin calcium mediated oligomerization

We measured the NMR parameters associated with changes in conformation, Ca^{2+} binding and oligomerization. Some studies showed that adding calcium to daptomycin led to line broadening of the ^{1}H-NMR signals due to chemical exchange between the Ca^{2+}-free and Ca^{2+}-bound daptomycin conformers and also by a change in T_2 relaxation due to oligomerization [26–28]. Firstly, we studied the effect of stepwise increment of Ca^{2+} (Ca^{2+} titrations) to the cyclic peptides, kynomycin and daptomycin, respectively. ^{1}H-NMR spectra were obtained using peptide: Ca^{2+} solutions in the range of 1:0 to 1:2.5 equivalents (Figs. 1, S1 and S2). As compared to daptomycin, the addition of Ca^{2+} to kynomycin caused a more severe linewidth disturbance (LWHH, line width at half height, $\nu_{1/2}$ in Hz), and many signals (i.e., see backbone NH region and CH_3 group in MeKyn13) merged with the baseline (See Fig. 1a and S1a), while daptomycin needed almost three times more Ca^{2+} than kynomycin to obtain comparable line broadening levels (Fig. 1). Moreover, to study the contribution of each residue separately, we monitored and mapped the visible (no overlapped) protons' LWHH changes of kynomycin and daptomycin (Figs. 1b, S1b and S2). MeKyn13 and Trp1 residues showed stronger LWHH disturbance in kynomycin than in daptomycin; this fact could suggest a local change in conformation around those regions in the presence of calcium. For each proton without overlap in the spectra we monitored and plotted the change in LWHH ($\Delta\nu_{1/2}$) during the Ca^{2+} titration (See Fig. S2) and fitted the sigmoidal curves to obtain the Ca^{2+} dissociation constants (K_D) (Table S1). The Ca^{2+} K_D value of kynomycin is found to be lower than that of daptomycin. The results suggest that kynomycin may be more subject to oligomerize in the presence of Ca^{2+} than daptomycin, and that Trp1 and MeKyn13 local conformation might be different.

When working with natural abundance $^{13}C/^{15}N$ samples, the use of 1D ^{1}H-NMR Ca^{2+} titrations in H_2O/D_2O allowed us to observe backbone NH signals and compare both peptides' local changes in conformation and oligomerization. To obtain a site-specific view of this effect, the 2D-NMR Ca^{2+} titrations were conducted. We run $^{13}C,^1$H-HSQC Ca^{2+} titrations with kynomycin, monitored the changes in the peptides' relaxation parameters and compared them to Ca^{2+} daptomycin titrations. In agreement with the 1D titrations, the presence of calcium also showed an increase in $^{13}C/^1$H peak linewidth together with a decrease in peak intensity. Again, compared to daptomycin, the addition of Ca^{2+} to kynomycin caused a more severe peak intensity disturbance (Fig. S3). However, a significant change in chemical shifts (CS) was not observed, so we correlated the process with slow exchange (oligomerization K_D values in the uM range). We monitored every peptide cross peak intensity, and as a result, similarly to the 1D titrations, a sigmoidal trend upon adding Ca^{2+} was observed (Fig. S4). Next, we estimated the Ca^{2+} concentration required to decrease each $^{13}C/^1$H peak intensity to 50% (we named it Ca^{2+}C50, see Fig. S5) for both peptides. The average

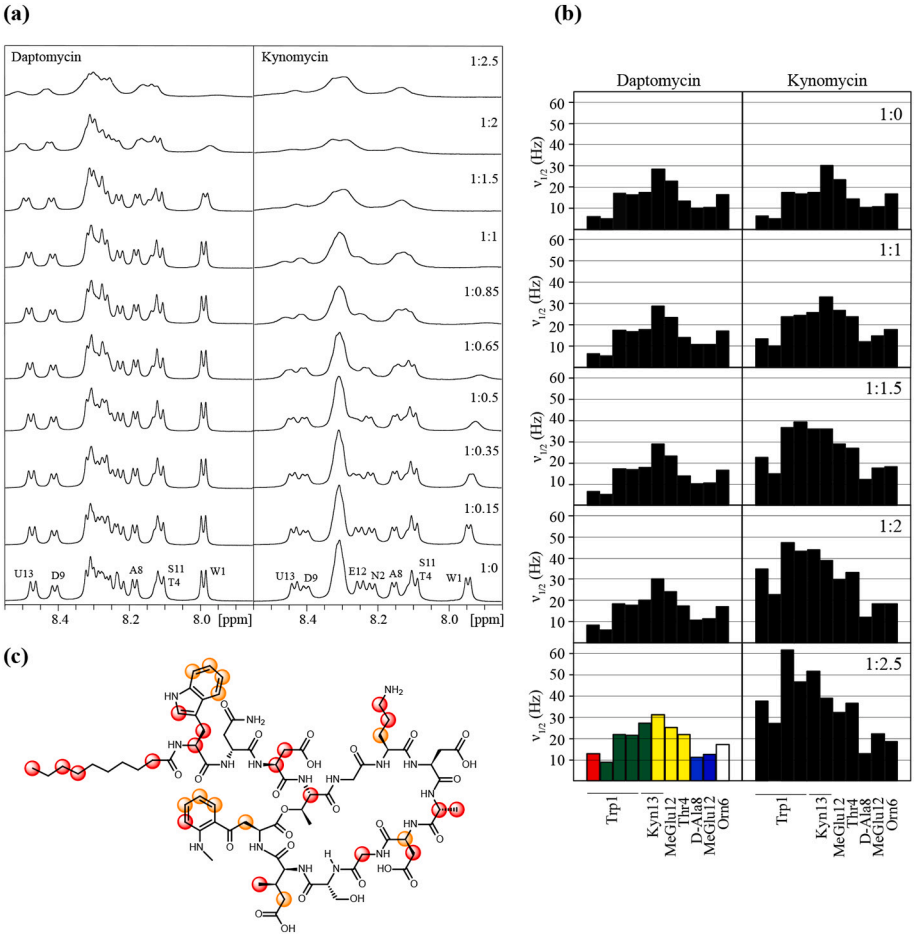

Fig. 1. Ca^{2+} dependent titrations. Titration of daptomycin and kynomycin with molar equivalents of Ca^{2+} (0 to 2.5 equivalents). Panel (a) shows the ^{1}H-NMR spectra of the backbone NH region. Resolved peptide resonances are highlighted. Panel (b) shows the line width at half height (LWHH, $\nu_{1/2}$ in Hz) of daptomycin (left) and kynomycin (right) against the molar equivalents of Ca^{2+} added (0 to 2.5; top to bottom plots). Red, green, yellow, blue and white coloured bands correspond to NH_{indole}, aromatic, Hβ, CH_3 and Hδ protons, respectively. Panel (c) shows kynomycin structure mapping the protons with $\Delta Ca^{2+}C50$ values ($Ca^{2+}C50_{Daptomyin}$-$Ca^{2+}C50_{Kynomycin}$, in mM) between 1 and 2 (orange spheres) and > 2 (red spheres).

daptomycin Ca^{2+}C50 value was calculated to be 7.39 mM, higher than for kynomycin (5.66 mM).

Next, we looked in detail at each amino acid contribution individually. We estimated the Ca^{2+}C50 difference between daptomycin and kynomycin for every CH signal (ΔCa^{2+}C50 values, in mM). This value highlights the peptide regions showing stronger perturbation in kynomycin compared to daptomycin. In detail, DAO (Decanoid acid chain), Trp1, Orn6, Asp3/9, Ala8, Gly10, MeGlu12 and MeKyn13 residues showed much higher ΔCa^{2+}C50 values in kynomycin (Fig. 1c). Moreover, the region concerning DAO, Trp1 and MeKyn13 shows more signals with higher ΔCa^{2+}C50 than the rest of the peptide. This result suggests that the local chemical environment around these areas in kynomycin may have changed, and may be now more buried into the oligomer structure than that for daptomycin.

To further study the Ca^{2+} dependent oligomerization, we compared the peptides' diffusion parameters during the Ca^{2+} titrations by acquiring Diffusion Ordered SpectroscopY (DOSY-NMR) experiments (Fig. 2, Fig. S6). While free kynomycin/daptomycin samples showed similar average diffusion coefficient values (*LogD* at −9.508 and −9.506 m^2s^{-1} respectively, apo-state), the presence of Ca^{2+} affected their oligomerization differently. For instance, in kynomycin the presence of 2.5-fold more of Ca^{2+} altered the diffusion values (See table in Fig. 2, *LogD* at −9.541 m^2s^{-1}, estimated to be *rH* of 8.5 Å by using modified Stokes–Einstein equation based on a sphere model [29]), whereas in daptomycin sample no significant effect was observed. These results were consistent with the ^1H and ^1H, ^{13}C-HSQC Ca^{2+} titration results, where less amount of Ca^{2+} was required for kynomycin oligomerization than for daptomycin. We sequentially increased the peptide: Ca^{2+} concentration to 1:4.5 ratio in order to saturate the peptide oligomer equilibria and measured the diffusion constants. At each Ca^{2+} adding point kynomycin showed higher diffusion constants than daptomycin (See Table in Fig. 2), and at the maximum Ca^{2+} concentration measured, kynomycin *rH* values were comparable to the estimated radii of gyration from the simulated tetramer (Rg_{MD}). Daptomycin *rH* values at maximum calcium concentration were found slightly lower than the simulated Rg_{MD}.

Next, we performed Ca^{2+} NMR titrations at different peptide concentrations. Analysed from the 2D-DOSY spectra of daptomycin and kynomycin at different concentrations in the absence of Ca^{2+} (See Fig. S7), both daptomycin and kynomycin diffusion values were constant, suggesting that under our experimental conditions, daptomycin and kynomycin remained in monomer state in the absence of Ca^{2+}.

From ^1H and 2D-DOSY Ca^{2+} NMR titrations, we found that kynomycin and daptomycin at low peptide concentrations behaved differently than at high peptide concentrations. In contrast to the titrations at high peptide concentrations (2 mM, Fig. 2), at low concentrations (0.5 mM), LWHH and diffusion values were unaffected using up to 1:19 peptide: Ca^{2+} ratios (See Figs. 2, S8A and C). However, spectra showed changes in ^1H CS and peak intensities (See Fig. S8B) suggesting that both peptides at low concentrations bind to Ca^{2+} in monomeric form. We monitored the changes in peak intensity during daptomycin an kynomycin Ca^{2+} titrations (Fig. S9) and observed similar trend with that at high peptide concentrations; signals coming from kynomycin showed a more severe peak intensity disturbance than daptomycin signals. Moreover, the estimated kynomycin Ca^{2+} K_D values were slightly lower than the ones from daptomycin at low peptide concentrations (See Fig. S10 and Table S2). The results altogether suggest that at both low and high peptide concentrations, kynomycin binding to Ca^{2+} is stronger than daptomycin.

To further confirm the Ca^{2+} binding results, we compared the binding affinity of kynomycin and daptomycin to an artificial lipid bilayer in the presence of Ca^{2+} by ITC (See Fig. 3). Our data showed that when the lipid bilayer was titrated against kynomycin in the presence of Ca^{2+}, kynomycin exhibited lower K_d values than with daptomycin [K_d of

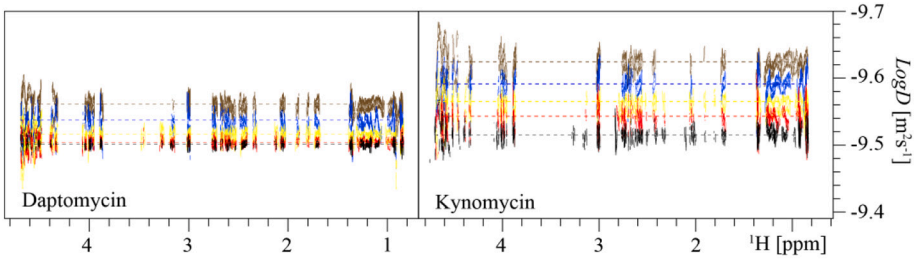

Peptide:Ca^{2+}	1:0	1:2.5	1:3	1:3.5	1:4.5	1:19
Daptomycin (2 mM) *LogD* ($m^2.s^{-1}$)	-9.506	-9.509	-9.521	-9.539	-9.565	nd.
Kynomycin (2 mM) *LogD* ($m^2.s^{-1}$)	-9.508	-9.541	-9.561	-9.596	-9.635	nd.
Daptomycin (0.5 mM) *LogD* ($m^2.s^{-1}$)	-9.508	nd.	nd.	nd.	nd.	-9.516
Kynomycin (0.5 mM) *LogD* ($m^2.s^{-1}$)	-9.505	nd.	nd.	nd.	nd.	-9.513
Daptomycin rH_{NMR} (Å)	7.9	7.9	8.1	8.4	9.0	8.0
Kynomycin rH_{NMR} (Å)	7.9	8.5	8.9	9.7	10.3	7.9
Tetramer Daptomycin Rg_{MD} (Å)					11.3	
Tetramer Kynomycin Rg_{MD} (Å)					11.5	

Fig. 2. Kynomycin and daptomycin oligomer size. 2D-DOSY spectra of daptomycin (left) and kynomycin (right) in the free state (in black), and after adding 2,5, 3, 3,5 and 4.5 increments of $CaCl_2$ (shown in red, yellow, blue and brown). The average diffusion coefficient (*LogD,* m^2s^{-1}, at 2 and 0.5 mM), hydrodynamic radii (*rH* Å, at 2 and 0.5 mM) and MD derived radii of gyration (Rg_{MD}, Å) values for each Ca^{2+} titration investigated are displayed.

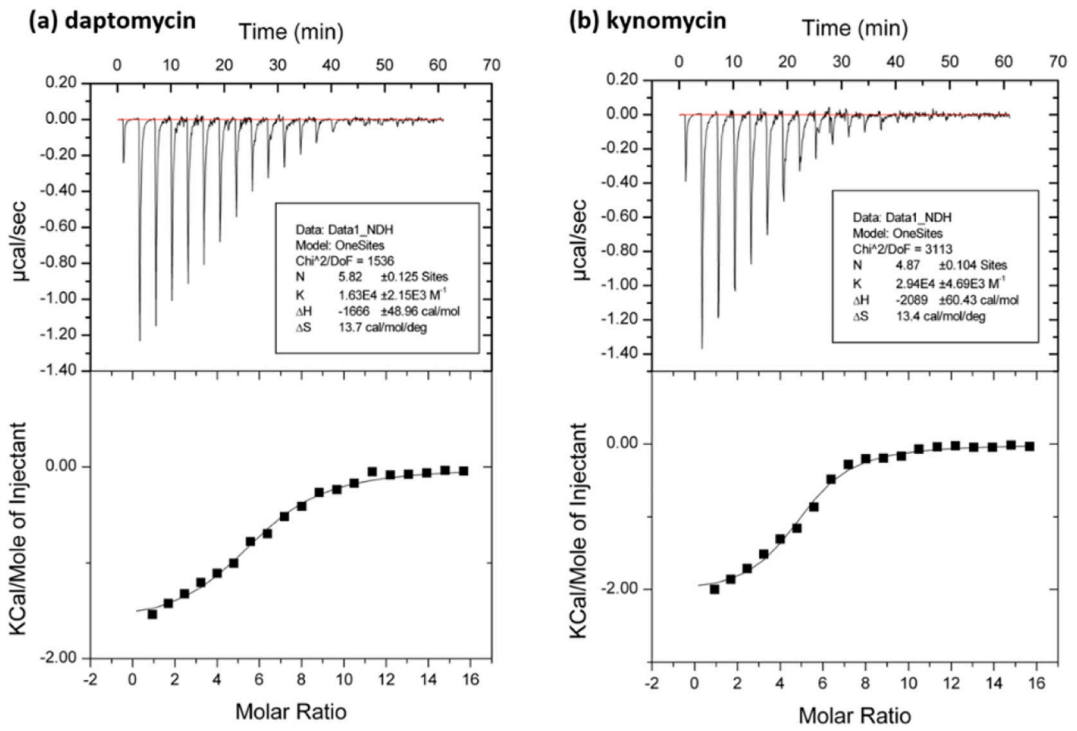

Fig. 3. Representative ITC traces and binding curves of (a) titration between 0.1 mM daptomycin and 7.5 mM lipid bilayer in the presence of 1 mM Ca^{2+} and (b) titration between 0.1 mM kynomycin to 7.5 mM lipid bilayer in the presence of 1 mM Ca^{2+}.

31.75 ± 0.04 μM ($n = 3$) for kynomycin and 71.60 ± 0.08 μM (n = 3) for daptomycin]. The results showed that kynomycin in the presence of Ca^{2+} binds tighter to the artificial lipid bilayer.

2.2. Peptide Ca^{2+} bound conformation

We analysed the structures of daptomycin and kynomycin in the absence (apo-form) and presence (oligomer-state) of Ca^{2+} from ^{1}H, ^{1}H-NOESY experiments. Both in the presence and absence of Ca^{2+}, when looking at the NH/Hα region, kynomycin and daptomycin eNOEs pattern and intensity were comparable (data not shown). Therefore, as same as reported for daptomycin [27,30–32], kynomycin showed no obvious differences in peptide backbone structure. Fig. 4 comprises the ^{1}H, ^{1}H-NOESY spectra region containing DAO, Trp1 and Kyn/MeKyn13 side chains. In detail, as shown in Fig. 4a, the absence of NOEs cross peaks in the DAO chain region suggests a high level of flexibility of this moiety for both daptomycin and kynomycin in the apo-state. These findings were consistent with previously reported for daptomycin in the apo-state [27]. However, in the presence of Ca^{2+} we observed local conformational changes around the DAO chain and several peptide side chains. The spectra of both compounds showed clear eNOEs between aromatic protons from Trp1 and Kyn/MeKyn13 and DAO. However, we found more eNOEs between MeKyn13/Trp1 and DAO in kynomycin than in daptomycin (Fig. 4b, c and Table S3). Moreover, we exclusively detected eNOEs between Trp1 and MeKyn13 in kynomycin: Ca^{2+} sample (Fig. 4d). These data suggest that Kyn13 methylation in kynomycin affects its side chain conformation to strengthen the contacts with Trp1 and the fatty acid chain in the oligomer state.

2.3. Kynomycin Ca^{2+} mediated tetramer oligomerization

To obtain more information about the Ca^{2+} dependent oligomerization of kynomycin, MD simulations of daptomycin and kynomycin tetramers were performed. Prior to the simulation, the distance between monomers was kept to >1.5 nm. For both peptides, after starting the simulations, the monomers started to become closer to each other due to thermal motion and the radius of gyration (Rg, Å) of the putative tetramer oscillated in a large range (15–45 Å). After 200–300 ns of simulation, the Rg curves reached a plateau which remained constant until the end of simulation (see Fig. S11). We calculated the average Rg values using the last 10 ns of the MD trajectories. The average Rg for daptomycin tetramer was 11.3 Å and for kynomycin tetramer 11.5 Å (see Fig. 2 and S11). Strictly, these two peptides exhibited similar geometric size in the tetrameric state. To further analyse the assembling process, we monitored the distances between monomers. Herein, we focus on the centres of mass of the backbone atoms forming the macrocyclic rings. From Fig. S12, we found a similar phenomenon for daptomycin and kynomycin. The peptides first form trimers and then between 240 and 300 ns the fourth monomer binds to the trimer to form the tetramer.

Next, we monitored the solvent accessible area (SASA) for each residue during the course of the simulation. A general decreasing trend in the SASA values for DAO, Trp1 and Kyn13/MeKyn13 was observed after the formation of the tetramers; which tended to get more buried in the oligomeric states. (Fig. S13A-B). This observation was further confirmed when comparing the average SASAs of these residues with those in the apo-form peptides (Table S4-S5). We observed exceptions for two DAO chains (B and D) in daptomycin and two DAO chains (B and C) in kynomycin, for which the SASA was either not significantly reduced or fluctuated until the end of the simulations. These results suggested that the alkyl chain showed intrinsic flexibility and allowed it to adopt different packing modes with other residues. Even though the high flexibility of the tetramer complexes during the simulation (See SD values in Table S4), we observed slightly different SASAs trend in some residues between daptomycin and kynomycin (i.e., see Trp1, Orn6, Asp7, Asp9, Glu12 and Kyn/MeKyn13 in Table S4). In contrast to these mentioned residues, the majority of other hydrophilic residues were more exposed to solvent with not strong SASAs change (Fig. S13A-B, and Table S5).

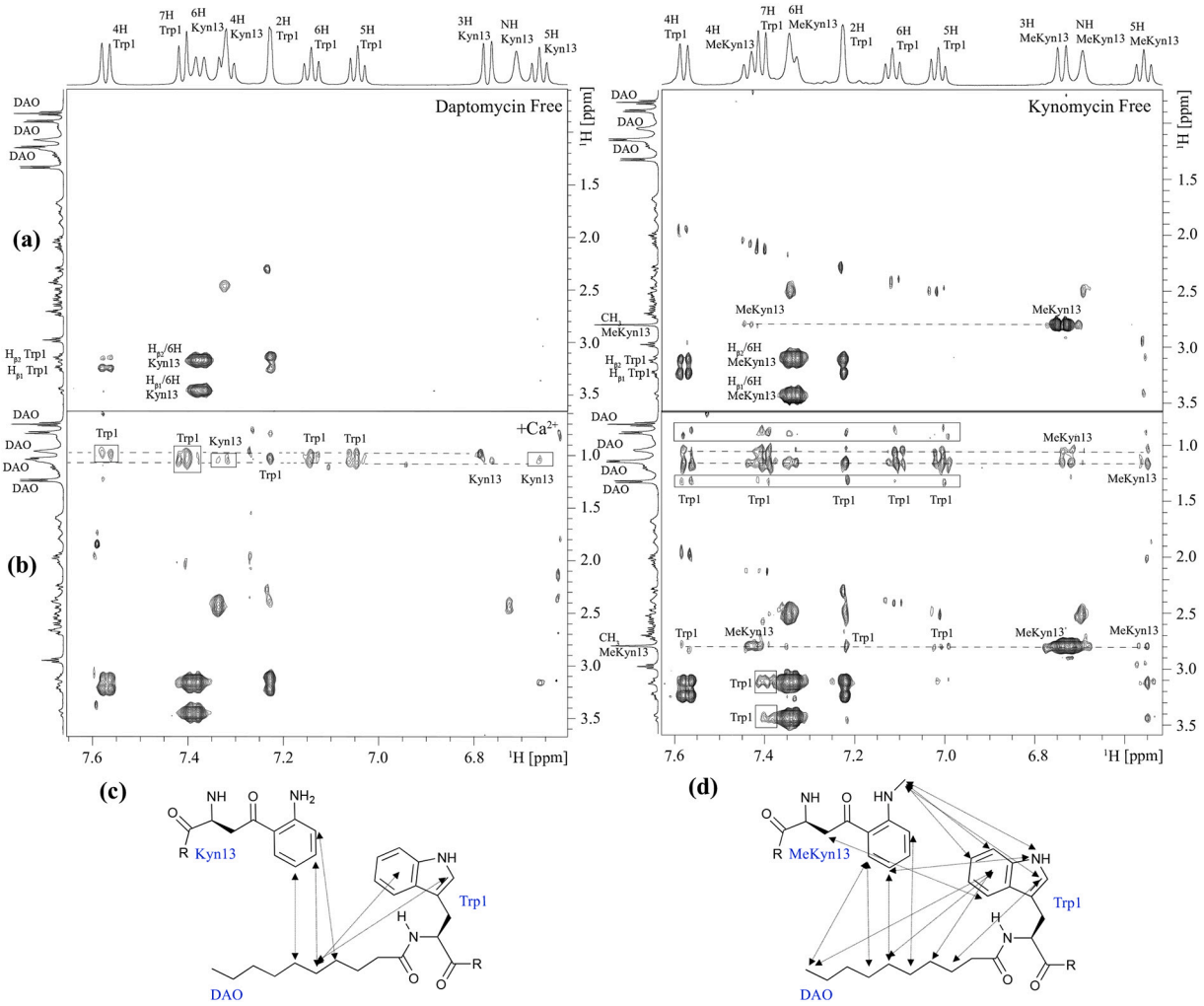

Fig. 4. Daptomycin and kynomycin Ca^{2+} bound conformation. Part of the ^{1}H, ^{1}H NOESY spectra of daptomycin (left) and kynomycin (right) in the apo-form (a) and in the presence of Ca^{2+} (b). Structures of Kyn/KynMe13, Trp1 and DAO for daptomycin (c) and kynomycin (d) showing eNOEs observed in (b) as double-headed arrows. Pertinent crosspeaks are annotated and highlighted in squares. List of observed eNOEs is shown in Table S3. DAO, Decanoid acid chain.

2.4. Core structures of daptomycin an kynomycin tetramers

We extracted the final frames of tetramers MD trajectories and visually analysed DAO and its interactions with Trp1 and Kyn/MeKyn13 (Fig. 5). In the case of daptomycin tetramer, we found both inter-molecular and intra-molecular interactions between the indole ring of Trp1 and the alkyl chain of DAO (In Fig. 5a, see monomers B and D for intra-molecular DAO-Trp1 interactions, and monomers A-B and D—C for inter-molecular DAO-Trp1 interactions). In the case of Kyn13, its interactions with DAO were mainly inter-molecular (see in Fig. 5A Kyn13 in monomer C and B). When analyzing the core of kynomycin tetramer (Fig. 5b) we observed both inter-molecular and intra-molecular interactions between DAO and Trp1/MeKyn13, which were found similar to daptomycin (for instance, Trp1 of monomer D was found in between DAOs of monomers A and D).

As observed during the SASAs analysis, both daptomycin and kynomycin tetramer complexes were flexible. Therefore, to completely understand the dynamics of the complex, we monitored the trajectories of key distances between residues DAO, Trp1 and Kyn/MeKyn13 during the simulation (Fig. S14A-J). Moreover, we extracted from the trajectories the DAO, Trp1, Kyn/MeKyn13 inter- and intra-residual distances which could show potential eNOEs (<3.5 Å, See Table S6).

Comparing the core structures of daptomycin and kynomycin tetramers during the simulations, we found a clear difference in Trp1 and Kyn/MeKyn13 local conformation preferences. Compared to daptomycin, kynomycin tetramer showed more regular inter- and intra-molecular packing between Trp1 and MeKyn13 (Fig. 5d, S14A-D, F—I and Table S6). The four monomers in kynomycin showed intra- and/or inter-molecular Trp1-MeKyn13 and MeKyn13/MeKyn13 packing with distances which could derive to eNOEs for the majority of simulation (See Fig. 5d, S14J and Table S6); however, in daptomycin most of those residues were found far to produce consistent eNOEs (Fig. 5c, S14E, Table S6). Moreover, in comparison to daptomycin, in kynomycin tetramer we observed an increase in number and frequency of Kyn13- and Trp1-DAO intrachain interactions with possible eNOE correlation (Table S6 and Fig. S14E, J). The results were in agreement with the $^{1}H,^{1}H$-NOESY derived eNOEs in the presence of Ca^{2+} (Fig. 5 and Table S3). The lipid DAO-MeKyn13 and -Trp1 eNOEs observed in kynomycin were principally coming from intramolecular interactions, whereas Trp1-MeKyn13 eNOEs were both inter- and intra-molecular. Therefore, we can suggest that kynurenine methylation in daptomycin changes its local conformation; these evidences might account for the improvement in oligomerization.

2.5. Kynomycin binding to Ca^{2+}

The binding of Ca^{2+} ions to each peptide monomer in daptomycin and kynomycin was analysed. Fig. 6 shows the tetramers of daptomycin

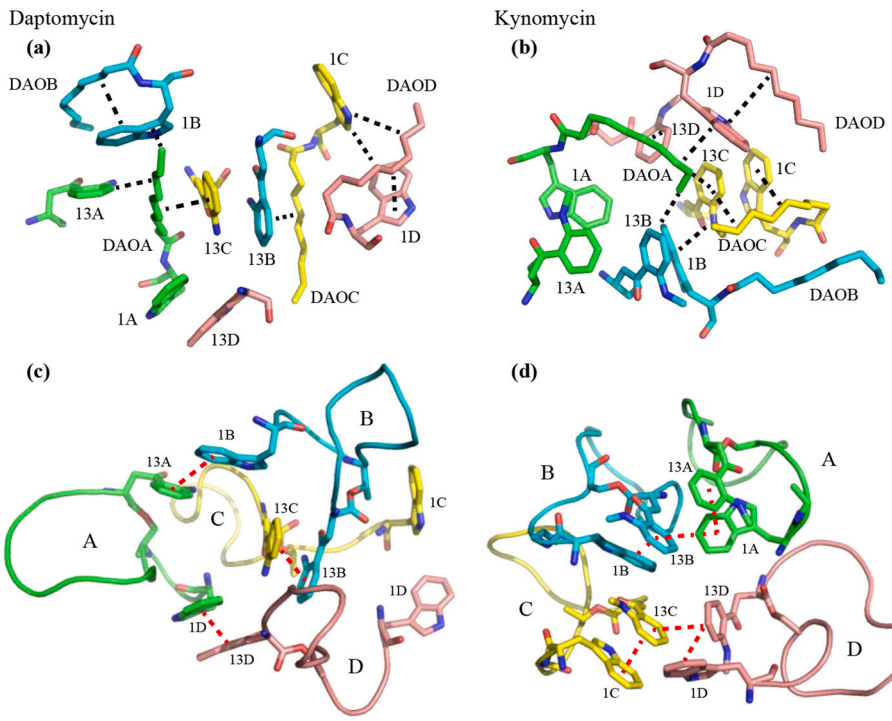

Fig. 5. Kynomycin and daptomycin core structures. Interactions between DAO, Trp1 and Kyn/MeKyn13 in (a, c) daptomycin and (b, d) kynomycin tetramers are shown. Peptide chains from monomers A, B, C, D are coloured in green, cyan, yellow and pink, respectively. Dashed lines in black show DAO-Trp1/Kyn/MeKyn13 and interactions and in red Trp1-Kyn/MeKyn13 and Kyn13 interactions. DAO lipid chain, Trp1 and Kyn/MeKyn13 are labelled with their residue numbers.

and kynomycin in the presence of calcium, and the plots show the closest distances between each Ca^{2+} and any oxygen atom of each monomer. The horizontal lines around 2.6 Å indicate the binding of Ca^{2+} to an oxygen of the peptide chain. In the case of daptomycin (Fig. 6, top panel), we observed Ca^{2+} number 1 (Ca1) steadily binding to monomer A until the end of the simulation when it also binds to monomer C. During the whole simulation, the Ca^{2+} number 2 was very active and it sequentially bound to dimers B/C, A/B, B/D and A/D (See Fig. 6, top panel). The binding of Ca4 to monomer D was also unstable. During the first 200–300 ns of simulation, Ca4 diffused away from monomer D and transiently bound to monomer B. Although it bound back to monomer D after 300 ns, it switched to monomer B after 450 ns. The only exception was Ca3 which simultaneously bound to monomers B and C shortly after the start of the simulation and the binding lasted until the end of the simulation.

In the case of kynomycin (Fig. 6, bottom panel), different Ca^{2+} behaviours were found. A simultaneous Ca1 and Ca4 interaction with two and three monomers was observed, respectively. Ca2 steadily bound to monomer D after 250 ns of simulation and occasionally bound to monomer A. The only exception was Ca3 which bound to monomer D shortly after starting the simulation and the binding lasted until the end (See Fig. 6, bottom panel). The results suggest that Ca^{2+} binds more stable to kynomycin tetramer than to daptomycin tetramer, which agrees with the Ca^{2+} affinity values calculated from the NMR Ca^{2+} titrations.

2.6. Kynomycin tetramer stability

Next, high-temperature MD simulations were performed to evaluate the stability of kynomycin and daptomycin tetramers [33]. We choose 100 °C (temperature sufficient to break intramolecular interactions) and simulate both tetramers in the presence of Ca^{2+}. As shown in Fig. 7, three dissociation events for daptomycin appeared as evidenced by the sudden jumps in the Rg curve. In contrast, the fluctuation magnitude of the Rg curve for kynomycin was much smaller and never reached Rg values higher than 15 Å, indicating the tetrameric structure of kynomycin was still maintained even at high temperatures. Therefore, we can suggest that the Ca^{2+}-bound kynomycin tetramer was more stable than that of Ca^{2+}-bound daptomycin.

3. Discussion

Structural modifications of small molecule antibiotics have led to many generations of new antibiotics with improved activities, while development of next generation-cyclic peptide antibiotics has not been successful. Recently, through comprehensive medicinal chemistry studies on daptomycin, we discovered kynomycin as a daptomycin derivative with improved antibacterial profiles. Herein, we showed that kynurenine methylation as in kynomycin changes daptomycin's key physicochemical properties which could be associated with its improved antibacterial activity. We found that kynomycin was more subject to oligomerize in the presence of Ca^{2+} than daptomycin and showed stronger contacts between the lipid tail and Trp1 and MeKyn13 residues. We observed that, compared to daptomycin, kynomycin tetramer was more stable and its Ca^{2+} affinity was higher.

The mechanism of action of daptomycin has been investigated extensively, and recent reports are following a similar path for its mode of action: daptomycin oligomerizes in the presence of Ca^{2+} and penetrates the membrane bilayer [7–12]. When inserted into the membrane, daptomycin will bind to phosphatidylglycerol and reassemble into channels causing membrane depolarization and consequently cell death. However, new theories have been proposed recently. For example, some studies suggest that daptomycin recruits essential cell division and peptidoglycan biosynthesis machinery components which will dramatically change cell morphology and disrupt cell wall biosynthesis leading to a breach in the membrane and cell death [14–16]. Moreover, details regarding how specifically some of these events occur remain uncertain: for example, whether daptomycin can oligomerize when in solution so that delivers a large peptide concentration to the cell membrane; whether those oligomers are Ca^{2+} free or Ca^{2+} bound, whether the

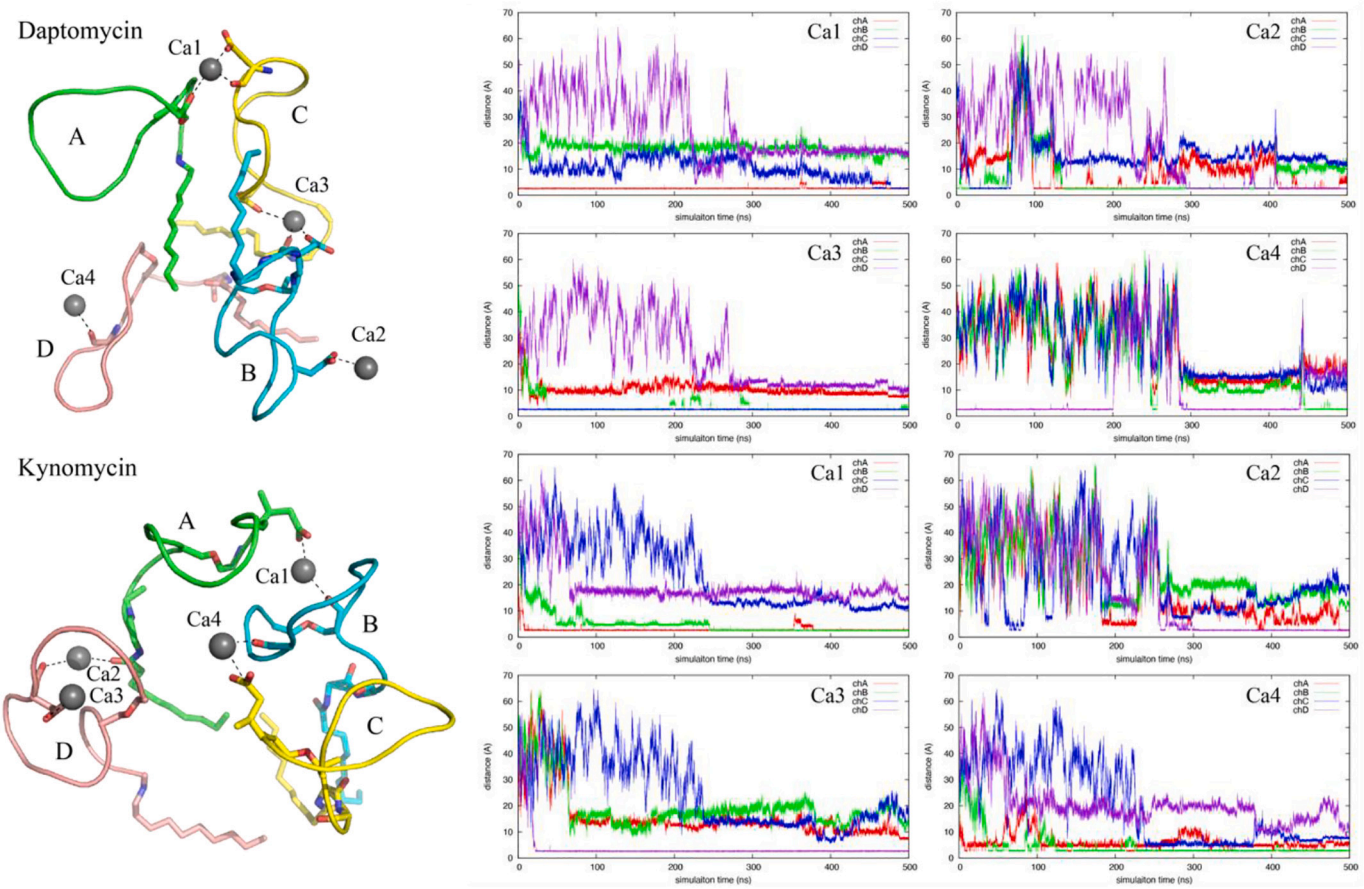

Fig. 6. Kynomycin and daptomycin binding to calcium. Representative daptomycin and kynomycin tetramer structures in the presence of calcium ions are shown. Calcium atoms Ca1-Ca4 are shown as grey spheres, and peptide chains A, B, C, D are coloured in green, cyan, yellow and pink, respectively. Distance monitoring between each Ca^{2+} atom and any oxygen atom of each daptomycin monomer (chA-chD, top plots, Ca1-Ca4) and kynomycin monomer (bottom plots, Ca1-Ca4) during the MD simulation is represented. (For interpretation of the references to colour in this figure legend, the reader is referred to the web version of this article.)

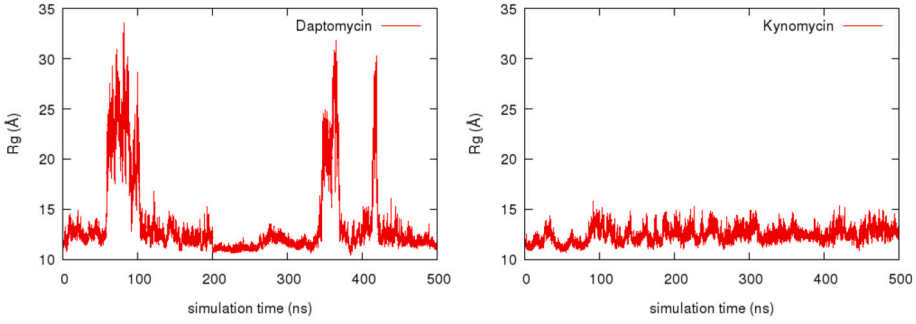

Fig. 7. High-temperature stability of kynomycin and daptomycin tetramers. Rg profiles (in Å) of Ca^{2+}-bound daptomycin (left) and kynomycin (right) tetramers at 100 °C during the simulation.

oligomer dissociates and penetrates the membrane bilayer and whether daptomycin forms well-defined oligomers in the membrane.

In our study, we do not try to reveal new findings in daptomycin's MOA, but we aim to understand in atomic detail the differences between kynomycin and daptomycin based on previous hypothesis raised about daptomycin MOA (which in our study, were Ca^{2+} binding and oligomer formation) by using NMR spectroscopy and MD simulations.

Previous works hypothesized that daptomycin requires calcium in the form of Ca^{2+} to form a micellar oligomer in solution [26,30], and that in the surroundings of the bacterial membrane where the peptide local concentration is higher, it can oligomerize [7–9]. This complex is required for daptomycin to bind to the bacterial membrane as a dissociated monomer or as Ca^{2+} bound-oligomer. Therefore, based on this hypothesis, we measured kynomycin's specific NMR parameters associated with changes in conformation, Ca^{2+} binding and mediated oligomerization and compared them to daptomycin's.

Some studies showed that adding Ca^{2+} to daptomycin led to line broadening of the ^{1}H-NMR signals [26–28]. This event was mainly caused by chemical exchange between the Ca^{2+}-free and Ca^{2+}-bound daptomycin conformers and also by a change in T_2 relaxation due to oligomerization. As we showed, compared to daptomycin, the addition of Ca^{2+} to kynomycin caused a more severe increase in linewidth and, specifically the methylated form of Kyn and Trp showed stronger disturbance. Upon the addition of Ca^{2+} we also observed stronger

changes in kynomycin's $^{13}C/^{1}H$ peaks intensity and diffusion coefficient values than to those of daptomycin. Moreover, by combining eNOEs and MD derived distances we observed in kynomycin that Kyn13 methylation strengthen its contacts with Trp1 and the fatty acid chain DAO in the oligomer state. The results suggest that kynomycin may be more prompt to oligomerize in the presence of Ca^{2+} than daptomycin, and that methylation at Kyn13 may stabilize even more the oligomer, by improving kynomycin inter- and intra-molecular interactions. The improvement in kynomycin's oligomer stability was further confirmed by the tetramer simulations at high temperature. We are also aware that Ca^{2+} concentration in serum is around 1.2 mM, but in order to estimate dissociation constants (K_D) and differentiate between kynomycin and daptomycin behaviour we needed to run a titration curve using higher and lower Ca^{2+} concentrations than 1.2 mM.

Few recent reports using small-angle x-ray scattering (SAXS), small angle neutron scattering (SANS) and fluorescence energy transfer (FRET; using NDB linked daptomycin) found that daptomycin may behave differently at different concentrations and in the presence or absence of Ca^{2+} [8,28,34]. Their results suggest that the relevant form of daptomycin in terms of its mode of action might be the monomeric form. For our study, we chose to use NMR spectroscopy because it is a powerful technique to study the dynamics of complex systems at atomic resolution, in solution without the need of fluorophore labelling. It can detect slight changes in relaxation and diffusion parameters due to changes in temperature, concentration, pH, binding to other molecules, and even more determine the regions in the molecule which are more or less perturbed. One of the main limitations in the use of NMR for our study was that to obtain a decent signal, we needed to use peptide concentrations in the low mM-high uM range. In the beginning of the study, for the Ca^{2+} titrations we used same peptide concentrations as previously reported for daptomycin NMR experiments (2 mM) [26,27], and in the same range as used for fluorescence [35,36], isothermal calorimetry (ITC) [7], and circular dichroism (CD) [7] studies. We also believe that following the "carpet model" theory for antimicrobial peptide membrane disruption [37], our experimental conditions might reflect the high local peptide concentration in the extracellular space near the bacterial membrane prior insertion. However, in agreement with previous reports [8,28,34], we found that kynomycin and daptomycin remained in monomer state at low concentrations both in the absence and presence of Ca^{2+}. Thus, we suggest that at this concentration, changes in relaxation parameters were exclusively caused by Ca^{2+} binding, and not by Ca^{2+} mediated oligomerization. Moreover, we found that at low peptide concentrations Ca^{2+} binds stronger to kynomycin than to daptomycin. These results were in agreement with the observations of Ca^{2+} binding from the MD simulations. Therefore, the results showed that kynomycin stronger K_D values (Table S1–2) were associated with an improvement in kynomycin's Ca^{2+} mediated oligomerization ability to a higher extent (high inter/intra-monomer interactions) and to Ca^{2+} binding to a lesser extent.

In conclusion, our results show that kynomycin's enhanced antibacterial activity can be due to the improvement in key physicochemical features like Ca^{2+} binding and Ca^{2+} mediated oligomerization. Due to the increasing number of recently discovered Ca^{2+} dependent peptide antibiotics, we believe that this NMR-MD based approach could be applied for the SAR determination of new analogues.

4. Material and methods

4.1. Daptomycin and kynomycin characterization by NMR

The NMR experiments for kynomycin and daptomycin chemical shifts assignment were performed on preparations at 2 mM in PBS buffer (pH 7.4) and 10% of D_2O (Cambridge Isotope Laboratories). ^{1}H NMR chemical shifts were referenced to external 3-trimethylsilyl-(2,2,3,3-D4)-propanoate (TSP, δ_H 0.00, Isotec Inc.). The temperature was set up at 298 K. Most of daptomycin ^{1}H NMR chemical shifts were available from the literature [30]. For the assignment of daptomycin and kynomycin $^{13}C/^{1}H$ NMR resonances, standard 1D ^{1}H NMR, 2D $^{1}H,^{13}C$-HSQC, $^{1}H,^{1}H$-COSY, $^{1}H,^{1}H$-TOCSY (70 ms of mixing time), and $^{1}H,^{1}H$-NOESY (mixing times 150 and 400 ms) experiments were carried out on a 500 Bruker Ascend spectrometer and 600 MHz Bruker Avance NEO Ultrashield spectrometer equipped with a TCI probe. $^{13}C/^{1}H$ chemical shifts assignments are shown in Table S7.

4.2. Daptomycin and kynomycin Ca^{2+} mediated oligomerization

The daptomycin and kynomycin samples for the initial ^{1}H Ca^{2+} titrations were prepared at 2 mM in PBS buffer and 10% or 100% D_2O (Cambridge Isotopes, Andover, MA). Ten samples were obtained from a single preparation; a high concentrated solution of $CaCl_2$ was added increasingly so that the molar ratio of daptomycin/kynomycin to Ca^{2+} ranged from 1:0 to 1:2.5 ($CaCl_2$ sample concentrations of 0, 0.3, 0.7, 1, 1.3, 1.7, 2, 3, 4 and 5 mM). For the ^{1}H-NMR Ca^{2+} titrations at low peptide concentrations, kynomycin and daptomycin samples were prepared at 0.5 mM in PBS buffer and 10% D_2O. Thirteen samples were obtained from a high concentrated solution of $CaCl_2$ keeping the molar ratio of daptomycin/kynomycin to Ca^{2+} ranged from 1:0 to 1:19 ($CaCl_2$ sample concentrations of 0, 0.035, 0.075, 0.15, 0.3, 0.6, 1.2, 2.4, 3.6, 4.8. 6, 7.2, and 9.6 mM).

All 1D ^{1}H-NMR spectra collected at 298 K were recorded using a 500 MHz Bruker Ascend spectrometer or a 600 MHz Bruker Avance NEO Ultrashield spectrometer equipped with a TCI probe. The spectra were acquired with 65 K data points, a spectral width of 15 ppm and a relaxation delay of 1 s. The spectra were all processed with the same phase correction and a line broadening of 1 Hz. The peak positions and linewidths ($\Delta\nu_{1/2}$, LWHH) were determined by fitting each resonance to a Lorentzian by using the "peakw" option in Bruker Topspin software (Bruker). ^{1}H-NMR chemical shifts were referenced to external 3-trimethylsilyl-(2,2,3,3-2H4)-propanoate (TSP, δ_H 0.00). Daptomycin and kynomycin ^{1}H-NMR signals with different FWHH during the titration are shown.

$^{13}C,^{1}H$-HSQC spectra were acquired with daptomycin and kynomycin samples at a concentration of 2 mM in D_2O PBS buffer. A solution of $CaCl_2$ was added increasingly so that the molar ratio of daptomycin/kynomycin to calcium ranged from 1:0 to 1:4.5 ($CaCl_2$ sample concentrations of 0, 0.3, 0.7, 1, 1.3, 1.7, 2, 3, 4, 5, 6, 7, 9 mM). Spectra collected at 298 K were recorded using a 600 MHz Bruker Avance NEO Ultrashield spectrometer equipped with a TCI probe. The spectra were acquired with 1024 × 128 data points for the direct and indirect dimensions, a spectral width of 9 × 220 ppm and a relaxation delay of 1.5 s. The spectra were all processed with the same phase correction and a line broadening of 1 Hz. The peak positions and intensities were determined by using the manual "pickpeak" option in Bruker Topspin software (Bruker) and normalized against the free daptomycin/kynomycin spectra. For every signal, the Ca^{2+} concentration to reach 50% of peak intensity inhibition was calculated ($Ca^{2+}C50$).

For the Ca^{2+} K_D estimation from linewidths or chemical shifts changes ($\Delta\nu_{1/2}$ or $\Delta\delta$) we treated data as reported for low affinity binding process [38–40]. In detail, if we consider Ca^{2+} as ligand A which binds to a molecule P (daptomycin/kynomycin), to form a 1:1 complex A–P, the dissociation constant, K_D will be defined by Eq. (1).

$$K_D = [A][P]/[AP] = k_{off}/k_{on} \quad (1)$$

All the fast-exchange NMR parameters (R; $\Delta\nu_{1/2}$ or $\Delta\delta$) can be cast in the following eq. (2) where α_f is the free Ca^{2+} mole fraction and α_b the bound fraction, ($\alpha_f + \alpha_b = 1$).

$$R_{obs} = \alpha_f R_f + \alpha_b R_b \quad (2)$$

where R_f and R_b are the corresponding NMR parameters of the free and bound states ($\Delta\nu_{1/2f}$, $\Delta\nu_{1/2b}$ or $\Delta\delta_f$, $\Delta\delta_b$), respectively. These equations can be simplified for an excess of the free ligand to obtain eq. (3).

$$[P]_T/(R_{obs} - R_f) = [A]_T + K_D/(R_b - R_f) \quad (3)$$

The variation of (R_{obs} - R_f) as a function of $[A]_T$ can be analysed in terms of two unknowns (R_b - R_f) and K_D. Then we plot R_{obs} - R_f versus $[A]_T$ allowing $1/(R_b - R_f)$ to be obtained from the slope of the sigmoidal titration curve (that is, the inflection point) and $K_D/(R_b - R_f)$ from the intercept on the y-axis. The equilibrium binding constant K_D can be determined from the behaviour of any one of the observable $\Delta\nu_{1/2}$ or $\Delta\delta$. Evidence for daptomycin/kynomycin-Ca^{2+} interactions can be seen in the binding-induced line broadening $\Delta\nu_{1/2}$ or chemical shift change $\Delta\delta$ in the peptide Ca^{2+} titrated NMR spectra, and the binding constant K_D can be determined, according to eq. (3) with $R_{obs} = \Delta\nu_{1/2obs}$ or $\Delta\delta_{obs}$.

4.3. Daptomycin and kynomycin Ca^{2+} mediated diffusion and oligomer size

For the 2D-DOSY Ca^{2+} titration experiments we used a 2 and 0.5 mM daptomycin/kynomycin sample in PBS 10% and 100% D_2O. 2D-DOSY experiments (standard pulse program "ledbpgp2s" and "stebpesgp1s") were acquired using molar ratios of daptomycin/kynomycin to Ca^{2+} ranged from 1:0 to 1:4.5 (0, 0.3, 0.7, 1, 1.3, 1.7, 2, 3, 4, 5, 6, 7, 9 mM) for 2 mM peptide concentration. Only Ca^{2+} titration samples with significant changes in diffusion (starting from 1:2.5 ratios) were shown. For 0.5 mM peptide concentrations, a ratio 1:19 peptide: Ca^{2+} was used (0, 9.6 mM). The spectra were performed at 298 K on a 500 MHz Bruker ASCEND or a 600 MHz Bruker Avance NEO Ultrashield spectrometer equipped with a TCI probe and experiments were run using 3 mm NMR tubes without spinning to minimize convection. The number of linear gradient steps was set to 32. The gradient recovery delay time was 0.2 ms and the eddy-current delay was 5 ms. Diffusion times and gradient pulse lengths were adjusted depending on the sample, (60–100 ms of diffusion time and gradient pulse length of 1.2–1.5 ms). The resulting NMR spectra were processed by Topspin software, and DOSY maps were generated using the AU DOSY module in Topspin. Averaged diffusion times (*Log D*) for each sample were calculated using the 'f1sum' macro in Bruker Topspin software. Kynomycin and daptomycin hydrodynamic ratio (*rH*, Å) were predicted using the Stokes-Einstein equation [29,41]:

$$D = kBT/6\pi\eta rH$$

where *D* is the diffusion coefficient (m^2s^{-1}), *kB* is the Boltzman's constant and η is the viscosity of the solution.

4.4. $^1H,^1H$-NOESY derived restrains

For both daptomycin and kynomycin, two samples (free and Ca^{2+}) were prepared. The initial free daptomycin/kynomycin samples were prepared at 2 mM in PBS buffer and 10% D_2O. The $CaCl_2$ concentrations used for the ^1H, ^1H-NOESY experiments were estimated based on the line broadening obtained in the ^1H-NMR spectra. To study the compounds conformation in the presence of Ca^{2+}, 4 and 1 mM of $CaCl_2$ were added to the free daptomycin and kynomycin samples; peptides at these concentrations showed similar level of line broadening. The upper bounds for the different eNOE levels were classified in two classes: high (≤1.8–2.7 Å), low (≤2.8 to 3.5 Å). The lower distance limits were taken as the sum of the van der Waals radii of two hydrogen atoms (1.8 Å). Phase sensitive ^1H, ^1H-NOESY experiments of dapyomycin and kynomycin were performed on a 500 MHz Bruker ASCEND spectrometer. The temperature was set up at 298 K. The spectra were acquired with a mixing time of 150 ms, a number of points 256 × 4 K in the F1 and F2 dimensions, a spectral width of 15 ppm and a relaxation delay of 1 s.

4.5. Isothermal titration calorimetry (ITC) assay

1-palmitoyl-2-oleoyl-*sn*-glycero-3-phosphocholine (POPC) and 1-palmitoyl-2-oleoyl-*sn*-glycero-3-phospho-(1′-*rac*-glycerol) (sodium salt) (POPG) were purchased from Avanti Polar Lipids, Alabaster, AL, USA. For the preparation of lipid bilayer/large unilamellar vesicles (LUVs, containing POPC and POPG in 1:1 ratio) POPC (0.025 mmol) and POPG (0.025 mmol) stock solutions in methanol and chloroform mixture were transferred to a round-bottom flask. The solvents were evaporated under a stream of argon and the lipid film was further dried under vacuum for 3 h. 1 ml of 10 mM HEPES buffer, 100 mM NaCl, pH 7.4 was used to hydrate the lipid film using slow agitation at room temperature. The resulting lipid suspension was then put into liquid nitrogen for 15 min, and incubated in a room temperature water bath for 15 min. The freeze-thaw cycle was repeated 5 times. The lipid bilayer suspension was diluted to the desired stock concentration and used immediately or stored at 4 °C and used within 2 days.

The ITC measurements were performed at 25 °C using a MicroCal iTC200 (Malvern). The reference cell contained water. The sample cell was filled with 0.1 mM of daptomycin or kynomycin in 10 mM HEPES buffer, 100 mM NaCl, 1 mM $CaCl_2$, pH 7.4. The sample syringe was filled with 7.5 mM POPC/POPG lipid bilayer in 10 mM HEPES buffer, 100 mM NaCl, 1 mM $CaCl_2$, pH 7.4. A total of 20 injections, 2 μl per injection, with 0.5 μl for the 1st injection was performed, with a stirring speed of 1000 rpm and 180 s spacing. Each experiment was performed in triplicate. Curve fitting was performed using Origin software package.

4.6. MD simulations of daptomycin or kynomycin: Computation methods

All MD simulations were run with Gromacs (version 5.1) . To account for the highly flexibility of daptomycin, we used the AMBER03w force field [43] and the TIP4P2005 water model [44], because this combination has been shown to well describe intrinsic disordered proteins/peptides [45]. All simulations were conducted under the constant number of particles, temperature and pressure (NPT) condition. The simulation temperature was set to 298.15 K or 398.15 K depending on the tasks of the simulations. The V-rescale thermostat [46] with a coupling constant 0.5 ps was used to control the simulation temperatures. The Parrinello-Rahman barostat [47] was used to control the pressure and the coupling constant was set to 5.0 ps. A time step of 2 fs was used throughout all simulations. The van der Waals (vdw) interactions were evaluated by twin-range cutoff method with the LJ potential truncated at 1.0 nm. The PME method was used to evaluate electrostatic interactions and the potential was cut off at 1.0 nm. Because the optimize_fft option of Gromacs was turned on, the precise setups for the vdw and PME cutoffs were slightly different among these simulations.

4.7. Daptomycin structures and force field parameters

The NMR structure 1XT7 [30] was used to derive force field parameters for the non-canonical amino acids of daptomycin and kynomycin. For D-amino acids, the force field parameters were copied from the corresponding L-amino acids in AMBER03w. According to the suggestion in the original paper [45], the phase term of the correction of the backbone ψ torsion (N-Cα-C-N_{i+1}) was reversed. The force field parameters for ornithine (Orn) and (2*S*, 3*R*)-3-methyl-glutamic acid (mGlu) were taken from previous work [48]. For the crosslinked threonine and kynurenine (Kyn) residues, we extracted them together and capped their amine groups with acetyl (Ace) groups and the carboxylate group with *N*-methyl (NMe) group. The resulting building block was subjected to geometry optimization by QM method (HF/6-31G(d)) with Gaussian 09 (revision D.01) [49]. Thereafter, the RESP method [50] was applied to derive atomic charges by using AMBER Tools 16 [51]. Atom types of atoms in these two residues were chosen from similar atom types in the AMBER03w force field. Parameters for bonding and non-bonding terms were copied from AMBER03w accordingly. For kynomycin, the same procedure was followed to derive force field parameters for non-canonical amino acids. We assumed that the methylation only affects the charge distribution on the Kyn residue and fixed the partial

charges on threonine. For the N-terminal lipid (denoted as DAO), we capped it with *N*-methyl amine group and derived atomic charges using the RESP method as well. The complete parameter sets of these residues are provided in the Supporting Information. In order to further investigate the applicability of the AMBER03w force field and the derived parameter sets mentioned above, the first structure of the NMR ensemble 1T5M [30] was subject to MD simulations, each lasting 500 ns. The trajectories were compared with the 1T5M ensemble and the 1XT7 structure. The backbone root mean squared deviation (RMSD) curves showed that all these conformations were sampled by the MD simulations when choosing the hit criteria as RMSD <2.0 Å.

4.8. Assembling and disassembling of daptomycin and kynomycin tetramers

For either cyclic peptide, four copies of the peptide were placed in a cubic box of 8.44*8.44*8.44 nm [44]. The box was solvated with TIP4P2005 water and Ca^{2+} ions were added at randomly chosen positions. The system was then neutralized by 100 mM NaCl. Two phases of equilibrium simulations were performed sequentially at NVT and NPT conditions and with temperature set to 298.15 K. Position restraints were applied to the backbone atoms of the four peptide molecules and the force constants of position restraints were set to 1000 kJ mol^{-1} nm^{-2} for all three Cartesian dimensions. After the equilibration simulations, position restraints are removed and the system was subject to 500 ns NPT simulation. For the disassembling of daptomycin and kynomycin tetramers, the last frame of the 500 ns assembling trajectory was extracted and heated to 398.15 K. After two phases of equilibrium simulations with position restraints on the backbone atoms of the peptide, a production simulation was propagated to 500 ns [33].

4.9. Analyses of MD simulation trajectories

All trajectories analyses were performed by using tools in the Gromacs package [42]. The radius of gyration (Rg_{MD}) and solvent accessible surface area (SASA) were calculated by using 'gyrate' and 'sasa' functions. The contacts between defined groups were evaluated as the minimum distance between two groups of atoms by the tool 'mindist'. The frequency of the potential $^1H—^1H$ eNOE correlation for DAO, Trp1, Kyn13 protons was calculated as the population (%P) of distances smaller than 3.5 Å during the last 200 ns (i.e., 300-500 ns) of the MD trajectories. To be specific, we picked the minimum distance at each time point from all proton pairs that were observed in the NOEs spectrum and then calculated the population of distances smaller than 3.5 Å.

Data availability

All data are contained within the manuscript.

Author information

These authors contributed equally: Pilar Blasco and Chunlei Zhang.

Funding and additional information

This work was supported by the Research Grants Council-Collaborative Research Fund (C7038-15G, C5026-16G), Research Impact Fund (R5011-18F), the Area of Excellence Scheme of the University Grants Committee of Hong Kong (AoE/P-705/16) and Croucher Foundation.

Declaration of Competing Interest

The authors declare that they have no conflicts of interest with the contents of this article.

Acknowledgments

The computations were performed using research computing facilities offered by Information Technology Services, the University of Hong Kong.

Appendix A. Supplementary data

Supplementary data to this article can be found online at https://doi.org/10.1016/j.bbagen.2021.129918.

References

[1] https://www.accessdata.fda.gov/drugsatfda_docs/nda/2003/21-572_Cubicin.cfm, 2021.
[2] R. Cha, W.J. Brown, M.J. Rybak, Bactericidal activities of daptomycin, quinupristin-dalfopristin, and linezolid against vancomycin-resistant Staphylococcus aureus in an in vitro pharmacodynamic model with simulated endocardial vegetations, Antimicrob. Agents Chemother. 47 (2003) 3960–3963.
[3] F.P. Tally, M. Zeckel, M.M. Wasilewski, C. Carini, C.L. Berman, G.L. Drusano, J. R. Oleson, Daptomycin: a novel agent for Gram-positive infections, Expert Opin. Investig. Drugs 8 (1999) 1223–1238.
[4] R.G. Hindes, S.H. Willey, G.M. Eliopoulos, L.B. Rice, C.T. Eliopoulos, B.E. Murray, R.C. Moellering, Treatment of experimental endocarditis caused by a beta-lactamase-producing strain of Enterococcus faecalis with high-level resistance to gentamicin, Antimicrob. Agents Chemother. 33 (1989) 1019–1022.
[5] S.J. van Hal, D.L. Paterson, I.B. Gosbell, Emergence of daptomycin resistance following vancomycin-unresponsive Staphylococcus aureus bacteraemia in a daptomycin-naïve patient—a review of the literature, Eur. J. Clin. Microbiol. Infect. Dis. 30 (2011) 603–610.
[6] A. Capone, V. Cafiso, F. Campanile, G. Parisi, B. Mariani, N. Petrosillo, S. Stefani, In vivo development of daptomycin resistance in vancomycin-susceptible methicillin-resistant Staphylococcus aureus severe infections previously treated with glycopeptides, Eur. J. Clin. Microbiol. Infect. Dis. 35 (2016) 625–631.
[7] R. Taylor, K. Butt, B. Scott, T. Zhang, J.K. Muraih, E. Mintzer, S. Taylor, M. Palmer, Two successive calcium-dependent transitions mediate membrane binding and oligomerization of daptomycin and the related antibiotic A54145, Biochim. Biophys. Acta Biomembr. 1858 (2016) 1999–2005.
[8] J.K. Muraih, A. Pearson, J. Silverman, M. Palmer, Oligomerization of daptomycin on membranes, Biochim. Biophys. Acta Biomembr. 1808 (2011) 1154–1160.
[9] T. Zhang, J.K. Muraih, E. Mintzer, N. Tishbi, C. Desert, J. Silverman, S. Taylor, M. Palmer, Mutual inhibition through hybrid oligomer formation of daptomycin and the semisynthetic lipopeptide antibiotic CB-182,462, Biochimica et Biophysica Acta (BBA) - Biomembranes 1828 (2013) 302–308.
[10] W.E. Alborn, N.E. Allen, D.A. Preston, Daptomycin disrupts membrane potential in growing Staphylococcus aureus, Antimicrob. Agents Chemother. 35 (1991) 2282–2287.
[11] J.A. Silverman, N.G. Perlmutter, H.M. Shapiro, Correlation of Daptomycin bactericidal activity and membrane depolarization in Staphylococcus aureus, Antimicrob. Agents Chemother. 47 (2003) 2538–2544.
[12] S.K. Straus, R.E.W. Hancock, Mode of action of the new antibiotic for gram-positive pathogens daptomycin: comparison with cationic antimicrobial peptides and lipopeptides, Biochim. Biophys. Acta Biomembr. 1758 (2006) 1215–1223.
[13] A.-B. Hachmann, E.R. Angert, J.D. Helmann, Genetic analysis of factors affecting susceptibility of Bacillus subtilis to Daptomycin, Antimicrob. Agents Chemother. 53 (2009) 1598–1609.
[14] A. Müller, M. Wenzel, H. Strahl, F. Grein, T.N.V. Saaki, B. Kohl, T. Siersma, J. E. Bandow, H.-G. Sahl, T. Schneider, L.W. Hamoen, Daptomycin inhibits cell envelope synthesis by interfering with fluid membrane microdomains, Proc. Natl. Acad. Sci. 113 (2016) E7077–E7086.
[15] J. Pogliano, N. Pogliano, J.A. Silverman, Daptomycin-mediated reorganization of membrane architecture causes Mislocalization of essential cell division proteins, J. Bacteriol. 194 (2012) 4494–4504.
[16] F. Grein, A. Müller, K.M. Scherer, X. Liu, K.C. Ludwig, A. Klöckner, M. Strach, H.-G. Sahl, U. Kubitscheck, T. Schneider, Ca2+-daptomycin targets cell wall biosynthesis by forming a tripartite complex with undecaprenyl-coupled intermediates and membrane lipids, Nature Communications 11 (2020).
[17] K.T. Nguyen, D. Ritz, J.-Q. Gu, D. Alexander, M. Chu, V. Miao, P. Brian, R.H. Baltz, Combinatorial biosynthesis of novel antibiotics related to daptomycin, Proc. Natl. Acad. Sci. 103 (2006) 17462–17467.
[18] J. Grünewald, S.A. Sieber, C. Mahlert, U. Linne, M.A. Marahiel, Synthesis and derivatization of Daptomycin: a Chemoenzymatic route to acidic Lipopeptide antibiotics, J. Am. Chem. Soc. 126 (2004) 17025–17031.
[19] J. Siedlecki, J. Hill, I. Parr, X. Yu, M. Morytko, Y. Zhang, J. Silverman, N. Controneo, V. Laganas, T. Li, J. Li, D. Keith, G. Shimer, J. Finn, Array synthesis of novel lipodepsipeptide, Bioorg. Med. Chem. Lett. 13 (2003) 4245–4249.
[20] J. Hill, J. Siedlecki, I. Parr, M. Morytko, X. Yu, Y. Zhang, J. Silverman, N. Controneo, V. Laganas, T. Li, J.-J. Lai, D. Keith, G. Shimer, J. Finn, Synthesis and biological activity of N-Acylated ornithine analogues of daptomycin, Bioorg. Med. Chem. Lett. 13 (2003) 4187–4191.
[21] Y. He, J. Li, N. Yin, P.S. Herradura, L. Martel, Y. Zhang, A.L. Pearson, V. Kulkarni, C. Mascio, K. Howland, J.A. Silverman, D.D. Keith, C.A. Metcalf, Reduced

pulmonary surfactant interaction of daptomycin analogs via tryptophan replacement with alternative amino acids, Bioorg. Med. Chem. Lett. 22 (2012) 6248–6251.
[22] N. Yin, J. Li, Y. He, P. Herradura, A. Pearson, M.F. Mesleh, C.T. Mascio, K. Howland, J. Steenbergen, G.M. Thorne, D. Citron, A.D.G. Van Praagh, L. I. Mortin, D. Keith, J. Silverman, C. Metcalf, Structure–activity relationship studies of a series of semisynthetic Lipopeptides leading to the discovery of Surotomycin, a novel cyclic Lipopeptide being developed for the treatment of *Clostridium difficile* -associated diarrhea, J. Med. Chem. 58 (2015) 5137–5142.
[23] D. Lin, H.Y. Lam, W. Han, N. Cotroneo, B.A. Pandya, X. Li, Structure-activity relationship of daptomycin analogues with substitution at (2S, 3R) 3-methyl glutamic acid position, Bioorg. Med. Chem. Lett. 27 (2017) 456–459.
[24] H.Y. Chow, K.H.L. Po, K. Jin, G. Qiao, Z. Sun, W. Ma, X. Ye, N. Zhou, S. Chen, X. Li, Establishing the structure–activity relationship of Daptomycin, ACS Med. Chem. Lett. 11 (2020) 1442–1449.
[25] H.Y. Chow, K.H.L. Po, P. Gao, P. Blasco, X. Wang, C. Li, L. Ye, K. Jin, K. Chen, E.W. C. Chan, X. You, R. Yi Tsun Kao, S. Chen, X. Li, Methylation of daptomycin leading to the discovery of kynomycin, a cyclic lipodepsipeptide active against resistant pathogens, Journal of Medicinal Chemistry 63 (2020) 3161–3171.
[26] K.S. Rotondi, L.M. Gierasch, A well-defined amphipathic conformation for the calcium-free cyclic lipopeptide antibiotic, daptomycin, in aqueous solution, Biopolymers 80 (2005) 374–385.
[27] D. Jung, A. Rozek, M. Okon, R.E.W. Hancock, Structural transitions as determinants of the action of the calcium-dependent antibiotic Daptomycin, Chem. Biol. 11 (2004) 949–957.
[28] J. Zhang, W.R.P. Scott, F. Gabel, M. Wu, R. Desmond, J. Bae, G. Zaccai, W.R. Algar, S.K. Straus, On the quest for the elusive mechanism of action of daptomycin: Binding, fusion, and oligomerization, Biochimica et Biophysica Acta (BBA) - Proteins and Proteomics 1865 (2017) 1490–1499.
[29] B.M. Schulze, D.L. Watkins, J. Zhang, I. Ghiviriga, R.K. Castellano, Estimating the shape and size of supramolecular assemblies by variable temperature diffusion ordered spectroscopy, Org. Biomol. Chem. 12 (2014) 7932–7936.
[30] L.-J. Ball, C.M. Goult, J.A. Donarski, J. Micklefield, V. Ramesh, NMR structure determination and calcium binding effects of lipopeptide antibiotic daptomycin, Organic & Biomolecular Chemistry 2 (2004) 1872.
[31] J.-Q. Gu, K.T. Nguyen, C. Gandhi, V. Rajgarhia, R.H. Baltz, P. Brian, M. Chu, Structural characterization of daptomycin analogues A21978C $_{1-3}$ ($_{D}$ -Asn $_{11}$) produced by a recombinant *Streptomyces roseosporus* strain, J. Nat. Prod. 70 (2007) 233–240.
[32] W.R.P. Scott, S.-B. Baek, D. Jung, R.E.W. Hancock, S.K. Straus, NMR structural studies of the antibiotic lipopeptide daptomycin in DHPC micelles, Biochim. Biophys. Acta Biomembr. 1768 (2007) 3116–3126.
[33] J.A. Lemkul, D.R. Bevan, Assessing the stability of Alzheimer's amyloid Protofibrils using molecular dynamics, J. Phys. Chem. B 114 (2010) 1652–1660.
[34] M.-T. Lee, W.-C. Hung, M.-H. Hsieh, H. Chen, Y.-Y. Chang, H.W. Huang, Molecular state of the membrane-active antibiotic Daptomycin, Biophys. J. 113 (2017) 82–90.
[35] J. Qiu, L.E. Kirsch, Evaluation of Lipopeptide (Daptomycin) aggregation using fluorescence, light scattering, and nuclear magnetic resonance spectroscopy, Journal of Pharmaceutical Sciences 103 (2014) 853–861.
[36] S. Kirkham, V. Castelletto, I.W. Hamley, K. Inoue, R. Rambo, M. Reza, J. Ruokolainen, Self-assembly of the cyclic Lipopeptide Daptomycin: spherical micelle formation does not depend on the presence of calcium chloride, ChemPhysChem 17 (2016) 2118–2122.
[37] Y. Shai, Mechanism of the binding, insertion and destabilization of phospholipid bilayer membranes by α-helical antimicrobial and cell non-selective membrane-lytic peptides, Biochimica et Biophysica Acta (BBA) - Biomembranes 1462 (1999) 55–70.
[38] J.K.M. Roberts, O. Jardetzky, Chapter 1 Nuclear magnetic resonance spectroscopy in biochemistry, in: New Comprehensive Biochemistry, Elsevier, 1985, pp. 1–67.
[39] R. Brüschweiler, D.A. Case, Characterization of biomolecular structure and dynamics by NMR cross relaxation, Prog. Nucl. Magn. Reson. Spectrosc. 26 (1994) 27–58.
[40] L. Verdier, J. Gharbi-Benarous, G. Bertho, N. Evrard-Todeschi, P. Mauvais, J.-P. Girault, Dissociation–equilibrium constant and bound conformation for weak antibiotic binding interaction with different bacterial ribosomes †, J. Chem. Soc. Perkin Trans. 2 (2000) 2363–2371.
[41] N. Giuseppone, J.-L. Schmitt, L. Allouche, J.-M. Lehn, DOSY NMR experiments as a tool for the analysis of constitutional and motional dynamic processes: implementation for the driven evolution of dynamic combinatorial libraries of helical strands, Angew. Chem. Int. Ed. 47 (2008) 2235–2239.
[42] S. Páll, M.J. Abraham, C. Kutzner, B. Hess, E. Lindahl, Tackling Exascale software challenges in molecular dynamics simulations with GROMACS, in: S. Markidis, E. Laure (Eds.), Solving Software Challenges for Exascale, Springer International Publishing, Cham, 2015, pp. 3–27.
[43] R.B. Best, J. Mittal, Protein simulations with an optimized water model: cooperative Helix formation and temperature-induced unfolded state collapse, J. Phys. Chem. B 114 (2010) 14916–14923.
[44] J.L.F. Abascal, C. Vega, A general purpose model for the condensed phases of water: TIP4P/2005, J. Chem. Phys. 123 (2005) 234505.
[45] S. Rauscher, V. Gapsys, M.J. Gajda, M. Zweckstetter, B.L. de Groot, H. Grubmüller, Structural ensembles of intrinsically disordered proteins depend strongly on force field: a comparison to experiment, J. Chem. Theory Comput. 11 (2015) 5513–5524.
[46] G. Bussi, D. Donadio, M. Parrinello, Canonical sampling through velocity rescaling, J. Chem. Phys. 126 (2007), 014101.
[47] M. Parrinello, A. Rahman, Crystal structure and pair potentials: a molecular-dynamics study, Phys. Rev. Lett. 45 (1980) 1196–1199.
[48] G.A. Khoury, J. Smadbeck, P. Tamamis, A.C. Vandris, C.A. Kieslich, C.A. Floudas, Forcefield_NCAA: *Ab Initio* charge parameters to aid in the discovery and Design of Therapeutic Proteins and Peptides with unnatural amino acids and their application to complement inhibitors of the Compstatin family, ACS Synth. Biol. 3 (2014) 855–869.
[49] M.J. Frisch, Frisch, M J Et al Gaussian 09, Revision D01, Gaussian, Inc., 2016.
[50] C.I. Bayly, P. Cieplak, W. Cornell, P.A. Kollman, A well-behaved electrostatic potential based method using charge restraints for deriving atomic charges: the RESP model, J. Phys. Chem. 97 (1993) 10269–10280.
[51] D.A. Case, R.M. Betz, D.S. Cerutti, T.E. Cheatham III, T.A. Darden, R.E. Duke, T. J. Giese, H. Gohlke, A.W. Goetz, N. Homeyer, S. Izadi, P. Janowski, J. Kaus, A. Kovalenko, T.S. Lee, S. LeGrand, P. Li, C. Lin, T. Luchko, R. Luo, B. Madej, D. Mermelstein, K.M. Merz, G. Monard, H. Nguyen, H.T. Nguyen, I. Omelyan, A. Onufriev, D.R. Roe, A. Roitberg, C. Sagui, C.L. Simmerling, W.M. Botello-Smith, J. Swails, R.C. Walker, J. Wang, R.M. Wolf, X. Wu, L. Xiao, P.A. Kollman, AMBER 2016, University of California, San Francisco, 2016.